

PREPARED FOR SUBMISSION TO JCAP

Testing the coupling of dark radiations in light of the Hubble tension

Zhiyu Lu,^{a,b} Batool Imtiaz,^{a,b} Dongdong Zhang,^{a,b} Yi-Fu Cai^{a,b}

^aDeep Space Exploration Laboratory/School of Physical Sciences, University of Science and Technology of China,
Hefei, Anhui 230026, China

^bCAS Key Laboratory for Researches in Galaxies and Cosmology/Department of Astronomy, School of Astronomy and Space Science, University of Science and Technology of China, Hefei, Anhui 230026, China

E-mail: zhiyulu@mail.ustc.edu.cn, batool24@mail.ustc.edu.cn,
don@mail.ustc.edu.cn, yifucui@ustc.edu.cn

Abstract. Self-interacting dark radiations (SI_{dr}) can have significant implications in the evolution of the universe, affecting the cosmic microwave background (CMB) and the clustering of large-scale structures. In this work, we analyze the implications of SI_{dr} on the CMB power spectrum and explore its potential in resolving the Hubble tension. SI_{dr} exhibits two distinct behaviors based on the interacting strength: strongly self-coupled and medium self-coupled. These behaviors are evident in the analysis of CMB data. According to Planck data, the dark radiation component consists of both free-streaming neutrinos and possible SI_{dr}. The total contribution from these components yields relativistic species with $N_{\text{eff}} = 3.046$. In the framework of universal coupling between dark radiations, a consistent value of $N_{\text{eff}} = 3.27^{+0.23}_{-0.31}$ is obtained. Additionally, this coupling results in an increase in the Hubble constant (H_0) to $70.1^{+1.3}_{-1.6}$ km/s/Mpc. However, when considering the number of free-streaming neutrinos as a parameter, the existence of SI_{dr} is not supported. This makes its fraction in radiation to be $R_x = 0.047^{+0.025}_{-0.053}$. Although the Hubble constant is still enhanced, it comes at the expense of a higher $N_{\text{eff}} = 3.52 \pm 0.25$. Our findings reveal that the ACT and SPT data provide support for the presence of SI_{dr}, particularly when considering a variable number of free-streaming species. In this case, SI_{dr} accounts for approximately 12.7% of the total radiation content. However, it is important to note that relying solely on SI_{dr} is insufficient to completely resolve the Hubble tension. Finally, we investigate the constraints on SI_{dr} imposed by future experiments, which improve the limits on scaled interacting strength $\log_{10} \tilde{G}_{\text{eff}}$ by a factor of 4.5 compared to the current constraints.

Contents

1	Introduction	1
2	Self-interacting dark radiations	3
2.1	Dark radiations Model	3
2.2	Impact on cosmological perturbations and CMB power spectra	3
2.3	Cosmological probe: The Hubble tension	6
3	Methodology	7
3.1	Data	8
3.2	Results	9
4	Fisher Forecast	13
4.1	Results	14
5	Conclusions and Outlook	15
A	Posterior distributions of all parameters	17

1 Introduction

The standard Λ CDM cosmological model has achieved remarkable success in describing the evolution history of the Universe, which includes structure formation and elemental synthesis. However, in the era of precision cosmology, it is crucial to assess both the theoretical and experimental self-consistency of Λ CDM model. Despite its overall success, there are indeed hints of tensions within the observed data.

One of the most pressing challenges is the discrepancy between the universe’s expansion rate as measured by the cosmic microwave background (CMB) experiments and local (low redshift) measurements [1], commonly referred to as the Hubble tension [2–4]. The observed discrepancy in the Hubble constant (H_0) between the Planck satellite’s estimation of $66.93 \pm 0.62 \text{ km s}^{-1} \text{ Mpc}^{-1}$ [5] and the measurement of $73.24 \pm 1.74 \text{ km s}^{-1} \text{ Mpc}^{-1}$ [1] by the SH₀ES collaboration amounts to more than 3σ [6]. This tension, if exists, strongly indicates the presence of new physics beyond the Λ CDM model.

Establishing a theoretical framework to resolve the Hubble tension is a daunting task. From the perspective of CMB power spectrum analysis, the precise determination of the acoustic peak angular scale θ_s is crucial, as it determines both the sound horizon at decoupling r_s and the distance D_A to the CMB surface of last scattering via $\theta_s = r_s/D_A$. One class of models aims to reduce the sound horizon in order to alleviate the Hubble tension. These models, known as early-time solutions, e.g., the early dark energy (EDE) model (see [7] for a comprehensive review) introduce an additional dark energy component that is active around the equality epoch and dilutes rapidly thereafter. Although EDE has shown promise in mitigating the Hubble tension, it has also introduced new challenges, such as worsening the S_8 tension and the coincidence problem [8, 9]. Moreover, some efforts have been made to investigate non-standard scenarios, e.g. dark matter-radiation interaction[10–12].

Another avenue for exploration lies in early dark radiations. In addition to the CMB photons, the Λ CDM model predicts the existence of a neutrino background that contributes to the radiation energy density ρ_r . This density can be expressed as:

$$\rho_r = [1 + \frac{7}{8}(\frac{4}{11})^{\frac{4}{3}} N_{\text{eff}}] \rho_\gamma, \quad (1.1)$$

where ρ_γ is the energy density of photons at a temperature of $T_\gamma = 2.725$ K, and $N_{\text{eff}} = 3.046$ [13] that accounts for the effective number of relativistic species within the standard model of particles. To reconcile the indirect measurements of H_0 from the CMB, Baryon Acoustic Oscillations (BAO), Type Ia Supernovae, and the direct measurements from the local distance ladder in physical theories, one may require $N_{\text{eff}} \simeq 3.95$ [14]. The additional contribution to N_{eff} could arise from unknown early dark radiations, such as sterile neutrinos [15, 16], self-interacting neutrinos [17, 18] and ultra-light axion-like fields [19, 20]. Conversely, the presence of additional N_{eff} enhances the damping tail of the CMB power spectrum [21], and similar effects can be analyzed through the spectral index n_s . This allows for compatibility between power law inflation and Planck data [22, 23].

The neutrino sector of the Standard Model (SM) of particle physics is a promising area to search for new phenomena that could help to pinpoint the ultraviolet completion of the SM. In the Λ CDM, the only dark radiations are the three flavors of free-streaming neutrinos [24], while terrestrial neutrino experiments have identified several anomalies that could potentially indicate the presence of new physics in the neutrino sector [25]. Cosmological data also indicates additional radiations [26]. This makes sterile neutrino one of the solutions to the anomalies as well as a candidate for SIdr [27–30].

Cosmological experiments, such as CMB polarization detection, provide valuable insights into the properties of dark radiations through two well-defined physical processes. Firstly, the total radiation energy density calibrates the Hubble rate and, consequently, the damping scale of CMB anisotropies [31]. Secondly, the presence of free-streaming relativistic particles, such as neutrinos, which introduce a phase shift and diminish the amplitude of the acoustic peaks observed in the CMB [32, 33]. In addition, it has also been shown in [34] that both the damping tail and phase shift allow us to jointly constrain the amount of free-streaming relativistic particles N_{eff} at CMB, and the number of relativistic particles that are fluid-like and tightly coupled, as opposed to free-streaming, parameterized by N_{fs} . Furthermore, the BAO feature in large-scale structure data also provides information about the phase of the acoustic oscillations that can supplement CMB constraints on N_{eff} [35–37].

In this study, our focus lies on the physics pertaining to the dark radiation component, where dark radiation is defined as the radiation other than photons. The main constituents of dark radiation includes free-streaming neutrinos (referred to as ν and predicted by the Λ CDM model) and self-interacting dark radiations (SIdr), denoted by the x . Notably, a specific model for SIdr involves the presence of sterile neutrinos interacting with active neutrinos. Within the context of the CLASS framework¹, the term "ultra-relativistic species" (ur) is often used interchangeably with free-streaming neutrinos [38]. We investigate how the latest CMB data can provide essential constraints on the SIdr properties and how the said scenario allows us to alleviate Hubble tension. In Section 2, we present the theoretical framework describing SIdr models and the physical impacts on the power spectra. In Section 3, we constrain the parameters with the latest CMB data. In Section 4, we summarize the Fisher information matrix

¹Ultra-relativistic Fluid Approximation.

method that we use in our forecasting analysis for next-generation experiments. Section 5 is dedicated to conclusion and outlook.

2 Self-interacting dark radiations

2.1 Dark radiations Model

The self-interactions among dark radiations intervened by a heavy mediator φ can be expressed as follows [28]:

$$\mathcal{L} \supset \lambda_\varphi \bar{x} x \varphi , \quad (2.1)$$

where λ_φ represents the coupling strength between the particle x and the mediator φ . This mechanism was originally proposed for self-interacting neutrinos [17]. In our study, we adopt this model and extend it to encompass all possible radiations by adjusting the statistical factor, relativistic species, and temperature [39].

We consider the case of dark radiations that can be effectively described as massless particles x . If the scalar field φ has a mass, we can approximate the interaction using a 4-Fermi effective operator when the temperature T_x drops below the mass of the scalar field. The effective Lagrangian can be written as:

$$\mathcal{L}_{\text{eff}} = G_\varphi \bar{x} x \bar{x} x , \quad (2.2)$$

where the coupling strength G_φ is inversely proportional to the square of the mediator mass m_φ , i.e., $G_\varphi \equiv \lambda_\varphi^2/m_\varphi^2$. In general, Eq. (2.2) describes a particle-particle scattering process.

It's interesting to note that SIdr will release the parameter space for the sterile neutrino (s), which is generated through the Dodelson-Widrow (DW) mechanism [40, 41]. The self-interacting potential will prohibit sterile neutrino existence until late time, protecting the Big Bang nucleosynthesis (BBN). The DW mechanism wouldn't change the energy density in the neutrino part because of the virtue of conservation [42]:

$$\frac{\partial}{\partial t} \sum_{s,\nu} f(p, T) - H p \frac{\partial}{\partial p} \sum_{s,\nu} f(p, T) = \mathcal{C}_{\text{SM}}[f] , \quad (2.3)$$

where f is the phase-space distribution and \mathcal{C}_{SM} is the collision term between neutrinos and standard model particles. On the right hand side of above equation, the effect of DW mechanism is canceled when we combine both active and sterile neutrinos altogether. Thus, a sterile neutrino generated in this way could potentially solve the anomalies in observations [41]. We would discuss the effect of sterile neutrinos generating from the DW mechanism on the N_{eff} in future work.

2.2 Impact on cosmological perturbations and CMB power spectra

In the standard model, neutrinos decouple from the photon-electron plasma at an early stage. Once decoupling occurs, they only interact under the influence of gravitational pull with standard model particles and become transparent to the universe [43]. All properties of free-streaming neutrinos can be parameterized by the effective relativistic degree of freedom N_{eff} and the free-streaming neutrinos fraction R_ν , which equals to 3.046 and 0.408 in Λ CDM respectively.

The deviation from the integer value of three occurring in N_{eff} is due to various factors in the early universe. For instance, neutrinos continue to interact with the primordial plasma

during electron-positron annihilation, which affects their temperature. Additionally, the energy dependence of neutrino interactions allows those at the high-momentum tail to interact with SM particles, affecting the energy spectrum of the neutrino gas [44]. After decoupling, the relativistic neutrino gas, without non-gravitational interactions, can be described by the effective number of neutrino species, N_{eff} . A high degree of confidence in the neutrino's effective degree of freedom consistent with 3.046 can provide robust evidence for the inclusion of Standard Model neutrinos. On the other hand, a value higher than 3.046 could indicate the existence of additional radiations.

The second parameter, R_ν , represents the fractional energy density contributed by free-streaming radiations, and it is given by

$$R_\nu = \frac{\rho_\nu^{\text{fs}}}{\rho_r} , \quad (2.4)$$

where ρ_ν^{fs} is the total free-streaming neutrino density and ρ_r is the total energy density in radiations including photons, neutrinos and possible dark radiations. Similarly, we define R_x as the energy fraction of the SIdr. Obviously, R_ν and R_x are complementary.

Assuming there are N_{ur} effective free-streaming neutrino species and N_x fermion-like SIdr relativistic species, the fractional density can be determined as:

$$R_\nu = \frac{\rho_\nu^{\text{fs}}}{\rho_\gamma + \rho_\nu + \rho_x} = \frac{\frac{7}{8}N_{\text{ur}}}{1 + \frac{7}{8}N_{\text{ur}} + \frac{7}{8}N_x\xi_x} , \quad (2.5)$$

In the second equation, we have used the fact that neutrinos are all free-streaming $\rho_\nu = \rho_\nu^{\text{fs}}$. The effective number of species [39] is

$$N_{\text{eff}} \approx N_{\text{ur}} + \left(\frac{4}{11}\right)^{-\frac{4}{3}} N_x \xi_x^4 . \quad (2.6)$$

Here $\frac{7}{8}$ stands for the statistical factor for fermionic particles and $\xi_x = T_x/T_\gamma$ is the temperature ratio of radiations to photons. Eq. (2.6) reveals the relationship between dark radiations temperature and flavors. As depicted in Figure 2, dark radiations can explain the entire neutrino contribution when $N_x = 3$, $\xi_x = (\frac{4}{11})^{1/3}$, and $N_{\text{ur}} = 0$, yielding $N_{\text{eff}} \approx 3.046$. However, it can also be interpreted with $N_x \approx 4$ and $\xi_x \approx 0.68$. Note that although Eq. (2.6) can't capture the contribution from non-instant neutrino decoupling, the error is well below the current experiment capacity.

In the standard model, we have three free-streaming neutrinos and no self-interacting radiations, i.e., $R_\nu^{\text{SM}} = 0.408$. Also, if all radiations are tightly coupled, then $R_\nu = 0$. Thus (N_{eff}, R_ν) can parameterize most properties of dark radiations through their background and perturbation features imprint on CMB².

The presence of free-streaming radiations perturb the CMB peaks and amplitudes. In the sub-horizon region and deep in the radiation-dominated epoch, the baryon density is negligible and the monopole of photon perturbation can be expressed as:

$$[\Theta_0 - \Phi](\tau) = [\Theta_0 - \Phi](0) \cos(kc_s\tau) - \frac{k}{\sqrt{3}} \int_0^\tau d\tau' [\Phi + \Psi](\tau') \sin[kc_s(\tau - \tau')] , \quad (2.7)$$

²If the dark radiations are coupled, the interaction strength is a key parameter as well.

where $(\Phi + \Psi)/2$ is the Weyl potential. Once the photons enter into the sound horizon, the Weyl potential decays to zero. Thus the decay potential is another source of the acoustic oscillation through the integral term, which is referred as the radiation driving effect [45, 46]. This extra source can carry a phase shift if the timing of the decay is modified. The amplitude of the radiation driving effect depends on the initial value of the Weyl potential

$$\Psi + \Phi = -(1 + \frac{5}{15 + 4R_\nu})\mathcal{R} , \quad (2.8)$$

where Φ, Ψ are the metric perturbations and \mathcal{R} is the comoving curvature perturbation. One can see that the decrease in fractional free-streaming radiations energy density enhances the radiation-driving effect through the initial value shift.

Another description for the phase shift can be illustrated as: free-streaming neutrinos travel with the speed of light through the photon-baryon plasma, which evolves as a fluid with a sound speed $c_s^2 \sim 1/3$. Hence, the free-streaming neutrinos gravitationally pull photon-baryon wavefronts slightly ahead of where they would be in the absence of neutrinos [47, 48], thus leading to the physical size of the sound horizon at last scattering r_* slightly larger than it would be otherwise. This phase shift is thought to be a robust signature of the presence of free-streaming radiations in the early Universe [34, 36].

The same idea can be applicable to the polarization multiples, through the equation [33]

$$\Theta_{P,\ell}(\tau_0) \simeq \frac{5}{18} \dot{d}_\gamma(k, \tau_{\text{rec}}) \dot{\kappa}^{-1}(\tau_{\text{rec}}) \left(1 + \frac{\partial^2}{\partial(k\tau_0)^2} \right) j_\ell(k\tau_0) . \quad (2.9)$$

We can notice that polarization multiples are proportional to the photon temperature fluctuations, i.e., $\Theta_{P,\ell} \propto \dot{d}_\gamma$, which causes them to be affected by neutrinos in the same way as the temperature does. Also, the time derivative of d_γ doesn't affect the phase-amplitude shift. As a result, the free-streaming neutrinos imprint a net phase and amplitude shift in the CMB power spectra. The shifted phase and amplitude are given by [32]

$$\phi_\nu \approx 0.19\pi R_\nu , \quad \Delta_\nu \approx -0.27R_\nu . \quad (2.10)$$

The presence of self-interaction between dark radiations stops them from free-streaming and delays the dark radiation decoupling time until a low redshift z_{dec} depending on the strength of the interaction. The free-streaming neutrino fraction R_ν is then decreased relative to Λ CDM. The amplitude of the SI_{dr} scenario thus is higher in the CMB temperature power spectrum compared with Λ CDM and the peaks are also shifted to higher ℓ [32]. These self-interaction dark radiations can be described by the following Boltzmann equation in the Newtonian gauge [49, 50]

$$\begin{aligned} \dot{\delta}_x + \frac{4}{3}\theta_x - 4\dot{\Phi} &= 0 , \\ \dot{\theta}_x + \frac{1}{2}k^2(F_{x,2} - \frac{1}{2}\delta_x - 2\dot{\Phi}) &= 0 , \\ \dot{F}_{x,\ell} + \frac{k}{2\ell+1}(\ell+1)F_{x,\ell+1} - \ell F_{x,\ell-1} &= \alpha_\ell \dot{\tau}_x F_{x,\ell} , \quad \ell \geq 2 , \end{aligned} \quad (2.11)$$

where $F_{x,\ell}$ is SI_{dr}'s perturbation expanded in multiple space, $F_{x,0} \equiv \delta_x$ and $F_{x,1} \equiv \frac{4}{3k}\theta_x$. In the above set of equations, α_ℓ are ℓ -dependent $\mathcal{O}(1)$ angular coefficients, depending on the nature of interaction model. Because of the energy and momentum conservation, $\alpha_\ell = 0$ for $\ell = 0, 1$ while, for $\ell \geq 2$, $\alpha_\ell \approx \mathcal{O}(1)$. The subsequent opacity from dark radiation self-scattering is $\dot{\tau}_x \propto G_{\text{eff}}^2 T_x^5$, determined by the interacting strength and temperature of SI_{dr}.

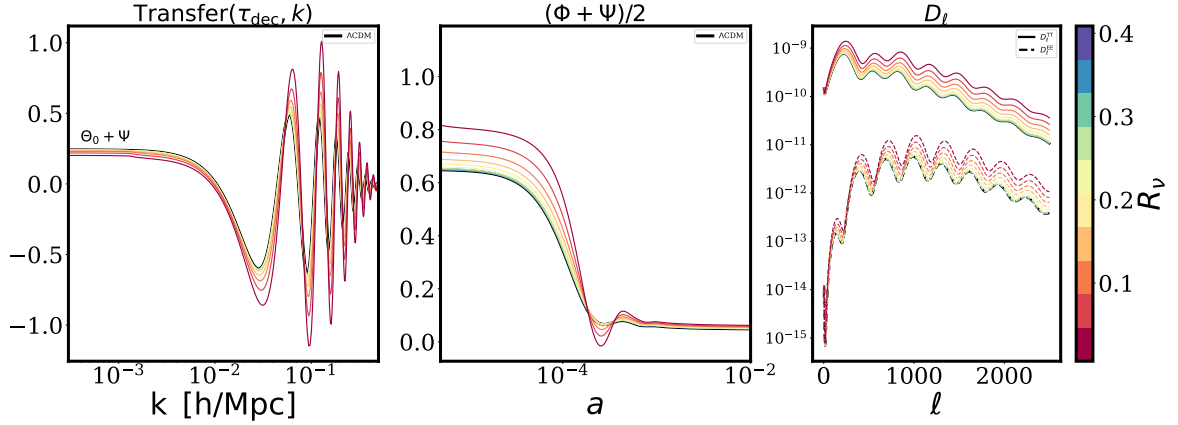


Figure 1. From left to right: The evolution of net monopole of the photon perturbation for various R_ν , the Weyl potential evolution at scale $k = 0.11/\text{Mpc}$ and the TT and EE power spectrum for different models are shown. The fraction of free-streaming neutrinos in the radiation is varied from 0 to 0.41. Note that the differences between SI_{dr} models and ΛCDM are deliberately amplified by a factor of ten to enhance visibility.

For a frequently interacting period, the high moments are suppressed, and these equations then behave like fluid. When $\dot{\tau}_x \rightarrow 0$, this makes Eq. (2.11) mimic free streaming radiations. The transition time is determined by G_{eff} . We use the publicly available modified CLASS [38] code CLASS_SInu³ to solve above set of equations.

In the Figure 1, we illustrate the evolution of the perturbation effects of net monopole, the Weyl potential and CMB TT and EE power spectra, by keeping $N_{\text{eff}} = 3.046$ fixed and varying the free-streaming fraction R_ν from 0 to 0.408. The left panel displays the variation in the net monopole of the photon perturbation as a function of R_ν . Compared to the ΛCDM scenario, the presence of SI_{dr} exhibit a higher amplitude of acoustic oscillations, and the peaks are shifted towards smaller scales. The middle panel demonstrates that the Weyl potentials have a larger initial value in scenarios with smaller R_ν . Consequently, the radiations driving effect is intensified, leading to the delay in their decay and resulting in a phase and amplitude shift in the photon transfer function. The resulting changes in the CMB TT and EE spectra are depicted in the right panel. We observe amplified amplitudes of the power spectra and a shift of the peak positions towards larger ℓ values as R_ν decreases. These effects reach their maximum as R_ν approaches 0.

2.3 Cosmological probe: The Hubble tension

By fine tuning the parameters R_ν , G_{eff} , and N_{eff} , one can manipulate the phases and amplitudes of the CMB spectra, creating room for a larger Hubble constant, as explained in Section 2.2.

The power of the SI_{dr} model becomes apparent when considering the peak of the CMB power spectrum, which can be determined using the equation [12]:

$$\ell_{\text{peak}} \approx (m\pi - \phi) \frac{D_A}{r_s}, \quad (2.12)$$

where m is an integer number referring to the index of the peak; ϕ is the phase as discussed in Eq. (2.10); r_s is the radius of the sound horizon. The comoving angular diameter distance

³https://github.com/anirbandas89/CLASS_SInu

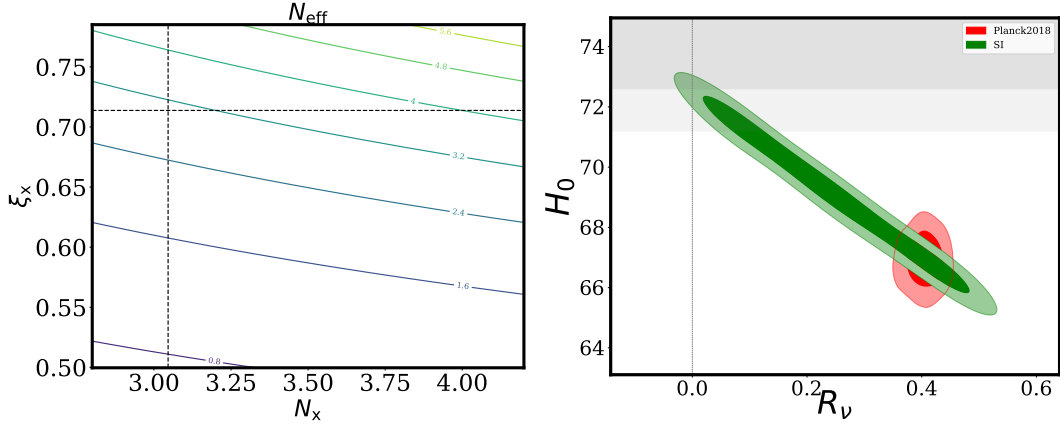


Figure 2. Left: The degeneracy relation between temperature ratio ξ_x and flavor number N_x . Right: The Hubble constant predicted by SI_{dr} as a function of R_ν , where N_{eff} is fixed to its Planck value. The gray area is the SH₀ES prediction for 1σ and 2σ .

D_A is defined as an integration from now to the last scattering surface z_{ls} :

$$D_A = \frac{c}{H_0} \int_0^{z_{\text{ls}}} \frac{dz}{[\rho(z)/\rho_0]^{1/2}}. \quad (2.13)$$

Here, $\rho(z)$ represents the energy density of the universe at redshift z , while ρ_0 corresponds to its present-day value. We can assert that H_0 is directly related to the function of phase suppressed by the sound horizon and late time physics involved in integration:

$$H_0 = \frac{m\pi - \phi}{\ell_{\text{peak}} r_s / \int_0^{z_{\text{ls}}} dz (\rho(z)/\rho_0)^{-1/2}}. \quad (2.14)$$

If SI_{dr} exists, then $\phi^{\text{SI}} < \phi^{\Lambda\text{CDM}}$. As a result, the numerator of Eq. (2.14) becomes smaller without introducing new energy components such as early dark energy or additional relativistic degrees of freedom. This naturally requires a larger H_0 while keeping the observed ℓ_{peak} fixed.

The Hubble constant proposed by SI_{dr} model compared with ΛCDM model is

$$\frac{H_0^{\text{SI}}}{H_0^{\Lambda\text{CDM}}} = \frac{\pi - 0.19\pi R_\nu^{\text{SI}}}{\pi - 0.19\pi R_\nu^{\Lambda\text{CDM}}}. \quad (2.15)$$

In Figure 2, we consider the Planck best-fit value of $H_0 = 66.93 \pm 0.62$, km/s/Mpc and $N_{\text{eff}} = 3.02 \pm 0.27$, as well as the SH₀ES measurement of $H_0 = 73.24 \pm 1.74$, km/s/Mpc (without considering covariance). Though we can easily see the ability of SI_{dr} in releasing the tension, i.e., $H_0 \approx 70$ km/s/Mpc within Planck result and with $R_\nu < 0.2$, it also shows the drawback of this scenario: without additional radiation part, SI_{dr} alone can't raise H_0 to 73 km/s/Mpc within 1σ Planck uncertainty.

3 Methodology

In this work, we consider a contribution of SI_{dr} to N_{eff} by introducing the temperature ratio ξ_x between dark radiations and photons as a free parameter. Since it is the value N_{eff} that

directly affects observations, the combination of ξ_x and the flavor of the dark radiations N_x introduces degeneracy, as discussed in Section 2.2, allowing for the possibility of additional sterile neutrinos or just three active neutrinos. Another free parameter in our analysis is the effective self-interacting strength $\log_{10} G_{\text{eff}}$, appearing in Eq. (2.11) through $\dot{\tau}_x$. Because of the degeneracy between G_{eff} and T_x in the differential optical depth, it is important to note that when comparing models with different ξ_x , the interacting strength should be scaled according to the relationship proposed by [51]:

$$\tilde{G}_{\text{eff}} = G_{\text{eff}} \left(\frac{T_x}{T_\nu} \right)^{5/2}, \quad (3.1)$$

where T_ν is the temperature of neutrino in Λ CDM.

Depending on whether we include the free streaming of ultra-relativistic neutrinos N_{ur} , we can realize either a universal coupling or a flavor-specific coupling. In the latter case, the standard neutrinos are assumed to have the temperature ratio $\xi_\nu = (4/11)^{1/3}$, and the number of additional ultra-relativistic neutrinos N_{ur} become a free parameter.

As discussed in Section 2.1, our results will primarily focus on the two derived parameters (R_ν, N_{eff}) instead of (N_x, N_{ur}) as these are the parameters that can affect observations. In our analysis, we assume massless radiations since the impact of Sldr's mass is considered negligible, validated by the study in Ref [51].

For our analysis, we employ the Markov Chain Monte Carlo (MCMC) method, using the publicly available code **Cobaya** [52]. We sample from the posterior distributions using the Metropolis-Hastings algorithm implemented in **Cobaya**, and we adopt the Gelman-Rubin convergence criterion [53].

3.1 Data

In our analysis, we make use of the following datasets:

- **Planck**: We utilize the full temperature and temperature-polarization power spectra measured by the Planck collaboration. The likelihood is low ℓ -TT from **Commander**, $2 \leq \ell \leq 29$; low ℓ -EE from **Simall**, $2 \leq \ell \leq 29$; high ℓ -TT from **PlikHM**, $30 \leq \ell \leq 2508$; high ℓ -TTTEEE from **PlikHM**, $30 \leq \ell \leq 1996$. Further details regarding these likelihoods can be found in [54].
- **CMB Lensing**: We consider the Planck reconstructed CMB lensing power spectrum [54]. The CMB lensing power spectrum probes structures over a broad range of redshift, with a peak at $z \approx 1 - 2$. The scale cuts used in the Planck lensing power spectrum likelihood include modes with $8 \leq L \leq 400$, for which non-linear corrections are negligible.
- **Riess2018a**: We include the local measurement of the Hubble constant by the Hubble Space Telescope, $H_0 = 73.48 \pm 1.66$ [55].
- **Pantheon**: We incorporate the Pantheon dataset, which is a compilation of Type Ia supernovae measurements [56].
- **BAO**: We include measurements of the BAO from the 6dF Galaxy Survey [57], SDSS MGS [58], and SDSS DR12 [59].

- **Others:** Additionally, we analyze the CMB power spectra data obtained from the Atacama Cosmology Telescope (ACT) DR4 [60, 61]. For this purpose, we utilize the likelihood implemented in the **pyactlike** package. As well as the South Pole Telescope (SPT) polarization measurements obtained from SPT-3G [62]. We employ the combination likelihood TT, TE, EE to constrain our model.

Our baseline parameter space consists of nine parameters: the neutrino interaction strength G_{eff} , the temperature ratio of the dark radiations ξ_x , the Hubble constant H_0 , the physical energy density for cold dark matter and baryons $\Omega_c h^2$ and $\Omega_b h^2$ respectively, the re-ionization optical depth τ_{reio} , the spectrum amplitude A_s , and the spectrum index n_s . Since BBN is affected by N_{eff} , we take Y_p as another free parameter for possible $N_{\text{eff}} \gg 3$. We also consider a model with an additional free parameter N_{ur} , representing the number of ultra-relativistic free-streaming neutrinos. Our baseline dataset includes Planck, Pantheon, BAO, and SH0ES, and we also cross-check the analysis by combining with ACT-DR4 and SPT-3G data.

3.2 Results

Our analysis explores two distinct interacting models depending upon their coupling strength: the strong-interacting model with $\log_{10} \tilde{G}_{\text{eff}} > -2.5$ and the medium-interacting model with $\log_{10} \tilde{G}_{\text{eff}} < -2.5$. The impact of these models on various cosmological parameters can be observed in Figure 3 and Figure 4. As a result of the parameter degeneracy present in the formation of the power spectrum, the value of $\log_{10} \tilde{G}_{\text{eff}}$ and R_ν affect parameters such as H_0 , A_s , n_s , τ , Ω_m , and N_{eff} .

In Figure 3, we have analyzed two cases depending upon free parameters. Firstly, the only additional free parameter taken into consideration, apart from the parameters in the Λ CDM model, is G_{eff} , denoted by G (corresponding to pink color) and the other one is considering two free parameters G_{eff} and N_{ur} , denoted by $G + R_\nu$ (in blue). We have also made the possible comparison with Λ CDM (in red). A direct effect one can expect is that, for the models with only SIdrs (without free-streaming radiations), the phase shift in Eq. (2.12) is canceled. To keep the observations unchanged, a larger H_0 is required. On smaller scales, this shift is enhanced by the spectral index n_s . Additionally, the SIdr induces an amplification of the amplitude, resulting the smaller spectrum amplitude A_s .

Figure 3 demonstrates that both G and $G + R_\nu$ consistently predict a scaled interacting strength. Notably, the evolution of SIdr remains unaffected by the presence or absence of free-streaming neutrinos. This consistency arises from their shared value of $\dot{\tau}$, as described by Eq. (3.2)

$$\dot{\tau}_x \propto G_{\text{eff}}^2 T_x^5 = \tilde{G}_{\text{eff}}^2 T_\nu^5, \quad (3.2)$$

The incorporation of local H_0 data strengthens constraints in the strong interacting regime, leading to a reduction in uncertainty. This reduction is attributed to the capability of the strong interacting strength to fully account for the observed increase in H_0 . However, in the medium region, achieving higher values of H_0 requires the inclusion of additional free-streaming neutrinos, which introduces additional uncertainty. Intriguingly, the analysis of the scaled interacting strength \tilde{G}_{eff} reveals that the $G + R_\nu$ model exhibits a preference for the medium interacting region over the strong case, as depicted in Figure 4. This preference supports the Λ CDM model over SIdr.

In the subsequent panels of Figure 3, it becomes evident that free-streaming neutrinos play a vital role, constituting the majority of the dark radiations with a value of $R_\nu \approx 0.392$.

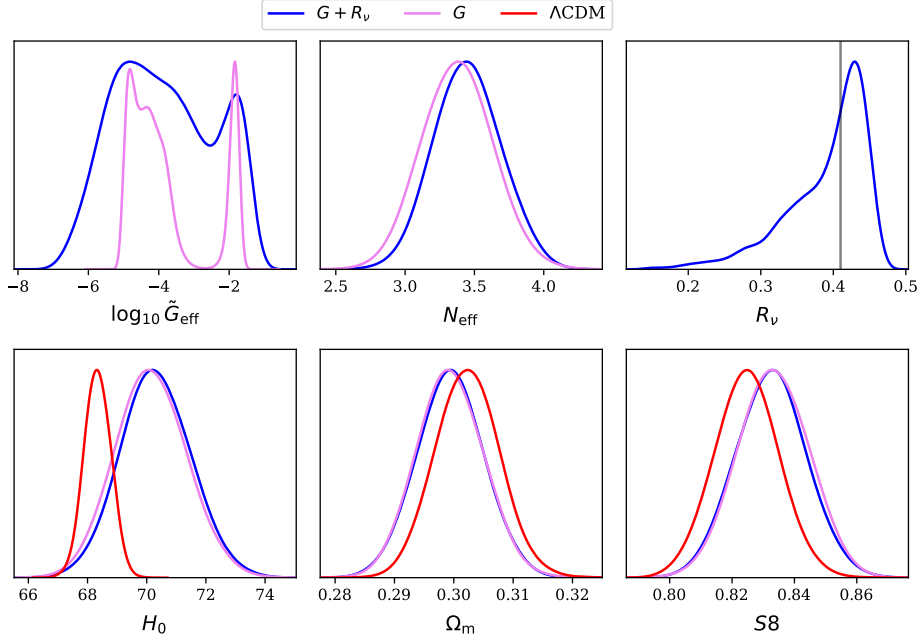


Figure 3. The one-dimensional posterior distributions of SIdr and SIdr plus free-streaming neutrinos under baseline data.

Considering free-streaming neutrinos as a free parameter with a uniform prior strongly favors their existence over SIdr. Furthermore, in the second row, although a similar increase in H_0 is observed, the underlying mechanisms differ significantly. One mechanism involves interacting dark radiations, while the other is driven by the presence of additional relativistic radiations. Therefore, SIdr has been considered inadequate for resolving the Hubble tension, as it fails to offer a comprehensive solution. Additionally, a similar outcome can be achieved by introducing additional free-streaming radiations with an approximate value of $\Delta N_{\text{eff}} \approx 0.22$.

Both models predict the same value of S_8 , providing support for the existence of tension in S_8 . Notably, the best-fit value of S_8 is higher than that predicted by ΛCDM due to the increased physical matter density, as illustrated in Figure 4.

Figure 4 illustrates the contour plots for different parameters. We observe that n_s and A_s are the parameters mostly affected by G_{eff} , while other parameters do not show obvious separated regions as expected in earlier paragraph. The significance of the strong interaction is smaller compared to the medium interaction in view of A_s and n_s . Most parameters are consistent with ΛCDM predictions, except the physical abundance of dark matter $\Omega_c h^2$, which determines the equality epoch. The increase of ω_c is a result of the increasing in N_{eff} as mentioned in [63]:

$$\Delta\omega_m \approx \omega_m^{\Lambda\text{CDM}} \frac{1 + \frac{7}{8}(\frac{4}{11})^{4/3} \Delta N_{\text{eff}}}{1 + \frac{7}{8}(\frac{4}{11})^{4/3} N_{\text{eff}}^{\Lambda\text{CDM}}}, \quad (3.3)$$

where Δ gives the difference compared to the value in ΛCDM .

Because most information of τ_{reio} comes from large-scale data, the parameter τ_{reio} remains unaffected by the existence of SIdr. Large-scale perturbations enter the horizon at a late time when the nature of the dark radiation doesn't matter⁴.

⁴At the late time, the self-scattering rate is far smaller than the universe expansion rate, thus can be taken

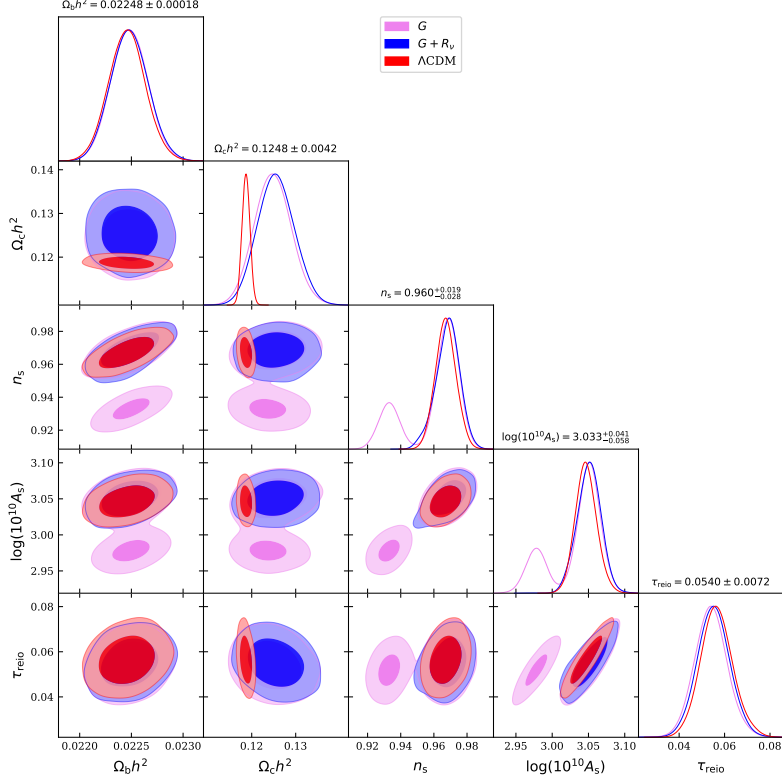


Figure 4. The two-dimensional posterior distributions of SIdr and SIdr plus free-streaming neutrinos models under baseline data.

In the right panel of Figure 5, we investigate the details of strong and medium self-interactions. It suggests that the parameter R_ν agrees with the Λ CDM in both cases. This implies the presence of free-streaming neutrinos necessary to account for the phase shift in the power spectra. It also shows that $G + R_\nu$ have a stronger tendency to Λ CDM, by allowing a fraction of SIdr approaching to zero, i.e., $R_x = 0.047^{+0.025}_{-0.053}$, Planck data thus favors free streaming neutrino more than SIdr.

We compare the best-fit power spectrum with the Λ CDM in terms of the cosmic variance. The oscillations observed in Figure 5 indicate a phase shift compared to the best-fit power spectrum of the Λ CDM. The cosmic variance can be calculated through the power spectrum

as free-streaming radiation

C_ℓ :

$$\sigma_{\text{CV}} = \begin{cases} \sqrt{\frac{2}{2\ell+1}} C_\ell^{\text{TT}} & TT ; \\ \sqrt{\frac{2}{2\ell+1}} C_\ell^{\text{EE}} & EE ; \\ \sqrt{\frac{1}{2\ell+1}} \sqrt{C_\ell^{\text{TT}} C_\ell^{\text{EE}} + (C_\ell^{\text{TE}})^2} & TE . \end{cases} \quad (3.4)$$

As shown in Figure 5, the model without free streaming neutrinos remains consistent with the best-fit power spectrum from the Planck data. The differences between the models are not apparent until the deep damping tail for $\ell > 2000$. Therefore, high-resolution experiments will play a crucial role in distinguishing between these two models. On the other hand, when free-streaming neutrinos are included, the peaks exhibit more out-of-phase oscillations as shown in Figure 5. Additionally, in the second panel, we observe that the

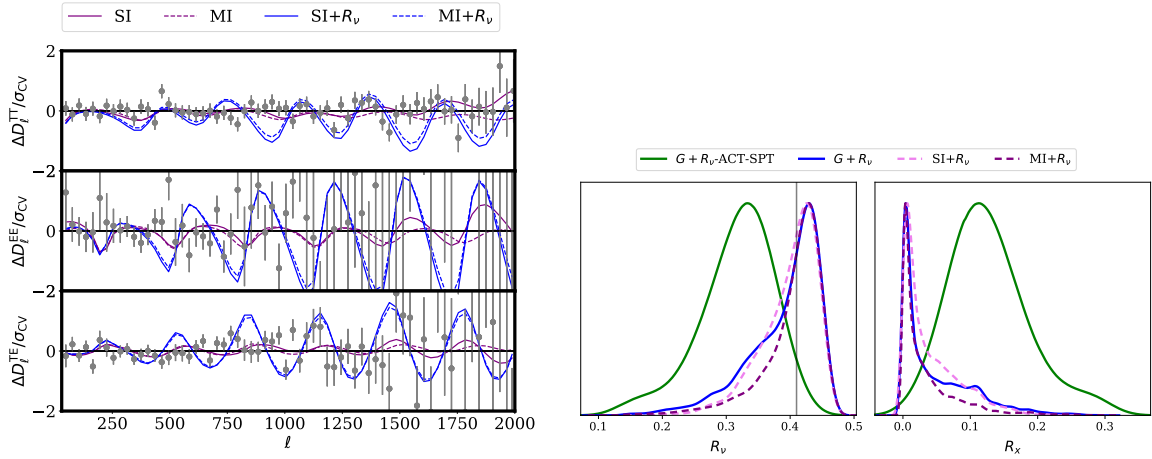


Figure 5. Left: the fractional difference in power spectra in terms of cosmic variance. We show the best fit result in both strong and medium interaction regimes. Right: The posterior one-dimensional distribution of the radiations fractions for different models and datasets. The gray vertical line is $R_\nu^{\text{SM}} = 0.41$, the ratio between free streaming neutrino and radiation in ΛCDM .

E-polarization data from Planck have limited constraints on the models, particularly in the case of free-streaming neutrinos.

When data from ACT and SPT are included, the existence of SIdr is favored, as shown in Figure 8. In G -ACT-SPT case, it has a similar result as the model constrained by Planck, except with no preference for medium interaction. The predicted N_{eff} is within Planck constraints. The combination of $G + R_\nu$ with ACT-SPT data makes the relativistic species go higher than the previous case as shown in Figure 4. Moreover, the fraction ratio for these neutrinos is smaller, i.e., $R_\nu \approx 0.317$. Thus, around 12% SIdr is allowed to exist as illustrated in the Figure 5 and Table 4. The predicted interacting strength for $G + R_\nu$ is bit higher. Because the increase in N_{eff} makes a stronger interaction which is required to observe the additional phase shift induced by free-streaming neutrinos. Finally, with additional relativistic species $\Delta N_{\text{eff}} = 0.25$ compared with curve G , $G + R_\nu$ -ACT-SPT predicts the largest $H_0 = 70.6 \text{ km/s/Mpc}$.

We have summarized all the results in Table 3 and Table 4. The χ^2 values have been calculated compared to the Λ CDM model using the baseline dataset. In all cases, the fitting to the CMB power spectra is worse. When comparing different models, we find that a better fit is achieved when the interacting strength decreases or when free-streaming neutrinos are included. This highly suggests none existence of SIdr, at least within the Planck scenario. Though, when the ACT-SPT data is included, SIdr plays an important role in getting a better fitting result. It is worth noting that the inclusion of SIdr leads to a higher value of N_{eff} which gives new challenges. Taking into account other datasets, we find that three cases have a better fit than the Λ CDM model, none of which correspond to the full coupling radiations. Additionally, the case with free-streaming neutrinos consistently performs better than the all-coupling case, i.e., $\Delta\chi_{G+R\nu}^2 < \Delta\chi_G^2$. In summary, within the range of $N_{\text{eff}} \sim 3$, the existence of SIdr is not favored. However, if we allow $N_{\text{eff}} > 3$, SIdr contributes around 10% of the total radiations.

4 Fisher Forecast

We have observed the significance of polarization data in constraining the properties of dark radiations. Thus, it becomes crucial to achieve a more precise detection of the CMB sky map, which improves the determination of peak amplitudes and phases, and reduces the level of noise. These advancements will greatly enhance our ability to constrain dark physics. In this section, we employ the Fisher forecast method to assess the potential of upcoming CMB experiments in constraining dark physics.

The Fisher matrix formalism is a widely used tool for predicting the statistical capabilities of future experiments in measuring cosmological parameters. It is defined as the expectation value of the second derivative matrix of the logarithm of the likelihood function with respect to the parameters of interest:

$$F_{ij} = - \left\langle \frac{\partial^2 \ln L}{\partial \theta_i \partial \theta_j} \right\rangle, \quad (4.1)$$

where the average is taken over all possible realizations of the data assuming a certain fiducial model. The errors on the parameters can be obtained from the inverse of the diagonal Fisher information matrix:

$$\sigma(\theta_i) = (F^{-1})_{ii}^{1/2}. \quad (4.2)$$

The Cramér-Rao bound states that the errors obtained from the Fisher information matrix represent the smallest achievable errors for unbiased estimators. In the case of a Gaussian likelihood, the components of the Fisher matrix are given by [64]:

$$F_{ij} = \sum_{\ell} \frac{2\ell + 1}{2} f_{\text{sky}} \text{Tr} \left(\mathbf{C}_{\ell}^{-1}(\vec{\theta}) \frac{\partial \mathbf{C}_{\ell}}{\partial \theta_i} \mathbf{C}_{\ell}^{-1}(\vec{\theta}) \frac{\partial \mathbf{C}_{\ell}}{\partial \theta_j} \right). \quad (4.3)$$

where f_{sky} is the sky coverage. and \mathbf{C}_{ℓ} is a matrix that containing various observables:

$$\mathbf{C}_{\ell} \equiv \begin{pmatrix} C_{\ell}^{TT} + N_{\ell}^{TT} & C_{\ell}^{TE} & C_{\ell}^{T\phi} & 0 \\ C_{\ell}^{TE} & C_{\ell}^{EE} + N_{\ell}^{EE} & 0 & 0 \\ C_{\ell}^{T\phi} & 0 & C_{\ell}^{\phi\phi} + N_{\ell}^{\phi\phi} & 0 \\ 0 & 0 & 0 & C_{\ell}^{BB} + N_{\ell}^{BB} \end{pmatrix}. \quad (4.4)$$

In this section, ϕ is the lensing potential [65]. We extend Eq. (4.4) by including the B-mode power spectrum. We assume a white-noise power spectrum $N_\ell^{XX'}$ for the effective noise, where $XX' \in \{TT, EE, TE, BB\}$, is given by;

$$N_\ell^{XX'} = s^2 \exp \left(\ell(\ell+1) \frac{\theta_{\text{FWHM}}^2}{8 \log 2} \right), \quad (4.5)$$

where θ_{FWHM} represents the experimental resolution, s is the instrumental noise in temperature, and $\sqrt{2}s$ is the noise in polarization. The noise for lensing potential is reconstructed according to [65]. The Fisher forecast is performed through a modification of the public code **Fishchips** [66].

In this study, we compare three categories of experiments: the current state-of-the-art CMB data, provided by the Planck satellite; the improved large-scale polarization CMB measurements by the scheduled experiment in Tibet⁵; the Stage-4 CMB experiment (CMB-S4) [79]. Details of the configurations we use is summarized in Table 1.

Experiment	ℓ -range	Noise s [$\mu\text{K-arcmin}$]	f_{sky}	θ_{FWHM} [arcmin]
Planck	2-2500	43	0.6	5
AliCPT	20-1000	8.6	0.1~0.4	11.0
CMB-S4	300-3000	1.0	0.4	1.5

Table 1. The experimental parameters used for the fisher analyses.

We assume equal ℓ -band coverage across different channels, including temperature, polarization-E, and lensing potential. Furthermore, we conducted an analysis to evaluate the potential improvement achieved by incorporating polarization B-mode data. However, our findings indicate that, even in CMB-S4 experiments, the contribution from polarization B-mode data is consistently limited, as illustrated in Figure 6 and Figure 7.

4.1 Results

The fiducial cosmology is based on the best-fit parameters in Section 3.2 for the model $G + R_\nu$ in the strong self-interacting regime.

First, we present the Fisher information for the Hubble constant across all ℓ bands, neglecting the covariance between different parameters (see Figure 6). On larger scales, the AliCPT could provides more information compared to Planck due to its lower noise level, depending on the sky coverage. But $f_{\text{sky}} < 0.2$ yields less information than Planck data. On smaller scales, the CMB-S4 experiment dominates because of its high resolution. The inclusion of polarization B-mode data does not significantly improve the results on H_0 while having $\mathcal{O}(0.1)$ contribution to the interacting strength $\log_{10} G_{\text{eff}}$ as indicated by the blue curves. For Planck data, the information is primarily concentrated in the middle bands $300 < \ell < 1800$, beyond which it decreases rapidly. Because of improved noise control in CMB-S4, it gives an abundant information in the far damping tail for $\ell > 1800$. We can proposed that CMB-S4 alone can not provide information about large-scales. Thus a combination of these three experiments will have the best capacity over the whole ℓ band.

⁵This is a CMB degree-scale polarimeter to be deployed on the Tibetan plateau, dubbed as the Ali CMB Polarization Telescope (AliCPT) [67–70]. Some related studies of this project can be found in [71–78] and references therein.

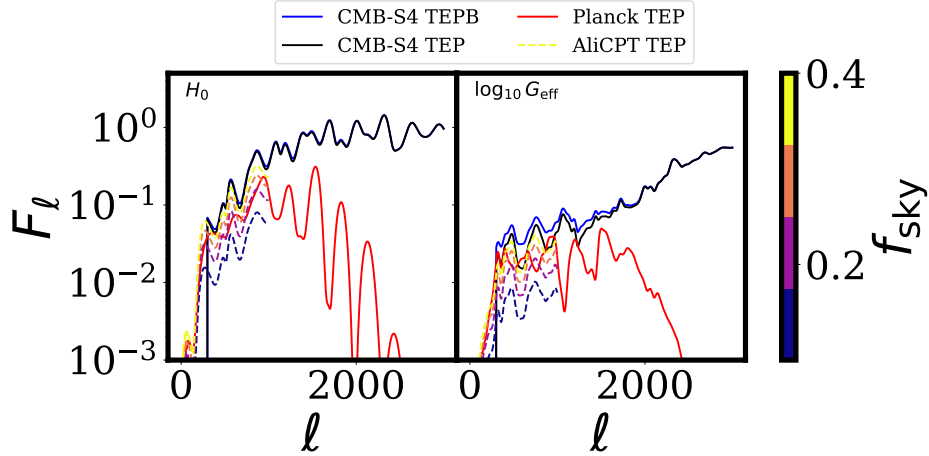


Figure 6. Fisher information according to the ℓ bands. For the AliCPT configuration, we have varied the sky coverage from 0.1 to 0.4 for the dashes lines.

Parameter	Planck-TEP	CMB-S4-TEP	CMB-S4-TEPB	combined-TEPB
$\log_{10} \bar{G}_{\text{eff}}$	0.64	0.15	0.14	0.13
H_0	0.35	0.15	0.14	0.11
N_{eff}	(-0.061, 0.019)	(-0.015, 0.0092)	(-0.014, 0.0069)	(-0.010, 0.0064)
R_ν	(-0.021, 0.028)	(-0.0084, 0.0094)	(-0.0083, 0.0091)	0.0071

Table 2. The values of parameters corresponding to different CMB experiments based on Fisher analysis.

From Figure 7 and Table 2, we can have a look over the predicted results. We show the analysis for several cases: CMB-S4 experiment using CMB temperature, polarization E, and lensing potential power spectrum, same configuration including polarization B power spectrum, a combination of Planck, AliCPT (we assume $f_{\text{sky}} = 0.4$), and CMB-S4 experiments using the whole CMB power spectrum. We use equal bands for different channels according to the corresponding experiment configuration in Table 1. Though including the B power spectrum has limited improvement on a single parameter, it helps to break the degeneracy between parameters. The combination experiments will have significant improvement on parameter constrain, e.g. the error on Hubble constant will decrease to 1/3 compared with the current constrains. We have concluded all the results in Table 2.

5 Conclusions and Outlook

Self-interacting dark radiations (SI_{dr}) can have significant impacts on universe evolution. When SI_{dr} enter the sound horizon, it remains coupled, thereby enhancing the radiation driving effects. Consequently, the phase and amplitude of these scales in the power spectrum are shifted. Therefore, SI_{dr} becomes a possible method to ease the tension between observations.

In this study, we introduced a temperature ratio as a free parameter, between dark radiations and photons, denoted as ξ_x , instead of specifying the integer flavors of dark radiations as in the previous work [80]. This parameter along with the interacting strength

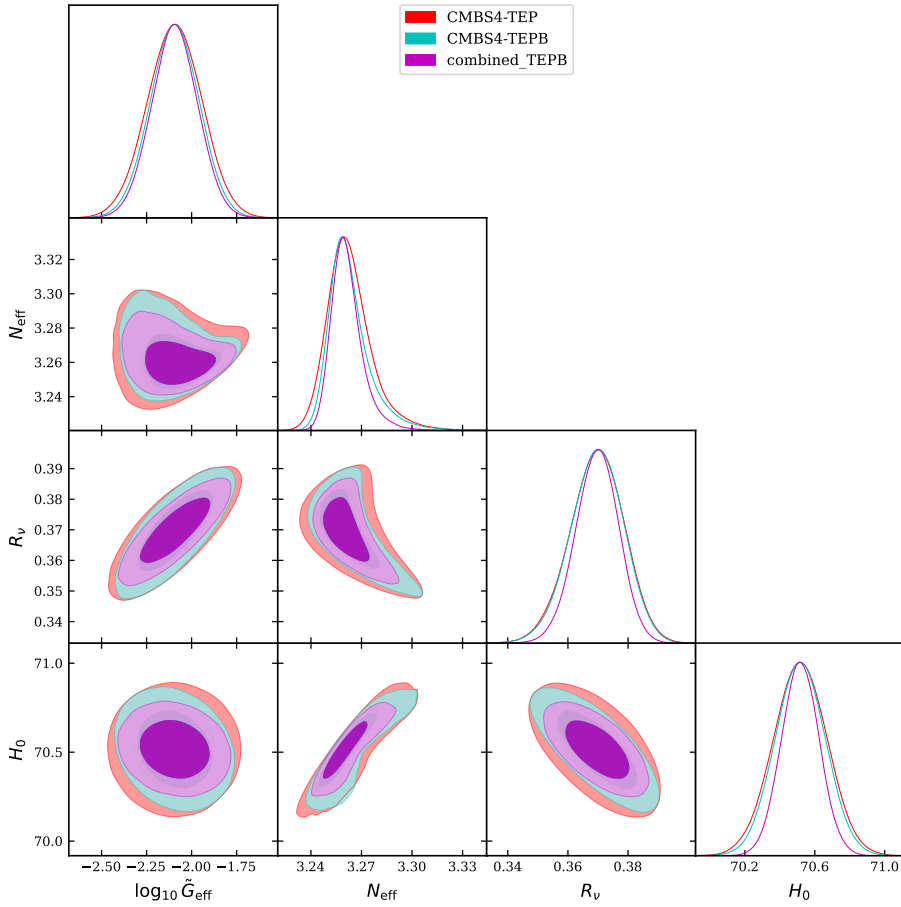


Figure 7. The Fisher forecast, using temperature, E polarization and lensing data for different experiments. We have taken the optimal case for the sky coverage in the AliCPT experiment, i.e., $f_{\text{sky}} = 0.4$. And N_{eff} and R_ν are derived parameters, thus they show non-Gaussian properties.

$\log_{10} G_{\text{eff}}$ captures all the properties of SI_{dr}. We considered two models to characterize the dark radiations content: SI_{dr} only and SI_{dr} + free-streaming neutrinos, denoted as G and $G + R_\nu$, respectively. The parameter R_ν represents the fraction of free-streaming neutrinos relative to all radiations and plays a crucial role in quantifying the effects of dark radiations on perturbation evolution. In the case of SI_{dr} only, we set $R_\nu = 0$, implying that all dark radiations are self-interacting. Our theoretical analysis reveals that without explicitly incorporating additional neutrino species, $N_{\text{eff}} = 3.02 \pm 0.27$, and an increased Hubble constant $H_0 = 69.3 \pm 2.0 \text{ km/s/Mpc}$ naturally emerged when all dark radiations were tightly coupled. However, within a 3σ confidence level (corresponding to a 99.7% probability), an upper bound of $H_0 < 72.9 \text{ km/s/Mpc}$ is predicted.

We utilize the latest CMB data from the Planck experiment, BAO data from SDSS, supernova (SN) data from Pantheon, and local H_0 measurements from SH₀ES to constrain the SI_{dr} model and address the Hubble tension. The results have been further validated using data from the Atacama Cosmology Telescope (ACT) and the South Pole Telescope (SPT).

The predictions obtained for the Λ CDM are consistent with all the datasets, and make an increase in the Hubble constant to approximately $H_0 \approx 70 \text{ km/s/Mpc}$. However, the

SI_{dr} model without free-streaming neutrinos are more consistent with Planck results for the parameters such as $N_{\text{eff}} = 3.23 \pm 0.25$. But it causes a degradation of the fits to both the CMB data and the baseline dataset. Moreover, the goodness of fit for a strong interaction result is not good compared to a medium interaction, whose limitation is Λ CDM. When considering the possibility of free-streaming neutrinos, the existence of SI_{dr} is strongly disfavored. Although incorporating SI_{dr} leads to an increase in the Hubble constant, it also increases the effective number of neutrino species (N_{eff}), suggesting that the increased H_0 is due to N_{eff} other than SI_{dr}. In other words, to achieve a higher H_0 , the model favors the inclusion of additional free-streaming neutrinos rather than SI_{dr}. As a cross-check, we analyze the SPT and ACT data, which provide more moderate results. These datasets supports the existence of approximately 12.7% SI_{dr} in the radiations component while raising N_{eff} to 3.52. However, the Hubble tension remained unresolved, with $H_0 = 70.6 \pm 1.3 \text{ km/s/Mpc}$. The full coupling case has always been disfavored by all the datasets as it leads to a degradation in the fits. Although ACT-SPT data leaves some room for the existence of SI_{dr}, it doesn't play the role that solves the Hubble tension. A comprehensive summary of all these results can be found in Table 3 and Table 4.

Finally, we employ a Fisher forecast analysis to predict future constraints on the SI_{dr} model. By including the polarization-B power spectrum, we find an $\mathcal{O}(0.1)$ level increase in information. This suggests that CMB-S4 experiment alone will improve the coupling strength $\log_{10} G_{\text{eff}}$ to $\mathcal{O}(4)$. Additionally, both AliCPT and Planck experiments enhance coupling strength by a factor of 4.57, considering $f_{\text{sky}} = 0.4$ for AliCPT.

A Posterior distributions of all parameters

Parameter	68%	Λ CDM	SG	MG	$G + R_\nu$
$\log(10^{10} A_s)$		3.047 ± 0.015	2.979 ± 0.016	3.051 ± 0.016	3.051 ± 0.017
n_s		0.9672 ± 0.0062	0.9330 ± 0.0066	0.9683 ± 0.0068	$0.9683^{+0.0078}_{-0.0064}$
$\Omega_b h^2$		0.02246 ± 0.00018	0.02250 ± 0.00018	0.02248 ± 0.00018	0.02248 ± 0.00018
$\Omega_c h^2$		0.11869 ± 0.00090	0.1238 ± 0.0044	0.1251 ± 0.0041	0.1255 ± 0.0042
τ_{reio}		0.0566 ± 0.0071	0.0519 ± 0.0072	0.0547 ± 0.0073	0.0552 ± 0.0073
H_0		68.34 ± 0.46	70.1 ± 1.3	70.2 ± 1.2	70.3 ± 1.2
$\log_{10} \tilde{G}_{\text{eff}}$		-	$-1.87^{+0.15}_{-0.077}$	$-4.29^{+0.41}_{-0.60}$	$-3.8^{+2.2}_{-1.8}$
N_{eff}		-	3.23 ± 0.25	3.43 ± 0.25	3.45 ± 0.25
Ω_m		0.3023 ± 0.0054	0.2979 ± 0.0055	0.2998 ± 0.0057	0.2994 ± 0.0057
$S8$		0.825 ± 0.010	0.832 ± 0.011	0.834 ± 0.012	0.833 ± 0.011
R_ν		0.408	0	0	$0.392^{+0.066}_{-0.023}$
R_x		-	-	-	$0.047^{+0.025}_{-0.053}$
$\Delta\chi^2_{\text{Planck}}$		-	6.3	4.0	3.2
$\Delta\chi^2_{\text{base}}$		-	2.6	-1.0	-2.1

Table 3. The best fit and 1σ error of the parameters. Here SG stands for strong interaction of all coupling case; similar to MG.

Acknowledgments

The authors thank Pierre Zhang for fruitful comments. This work is supported in part by the National Key R&D Program of China (2021YFC2203100), CAS Young Interdisciplinary

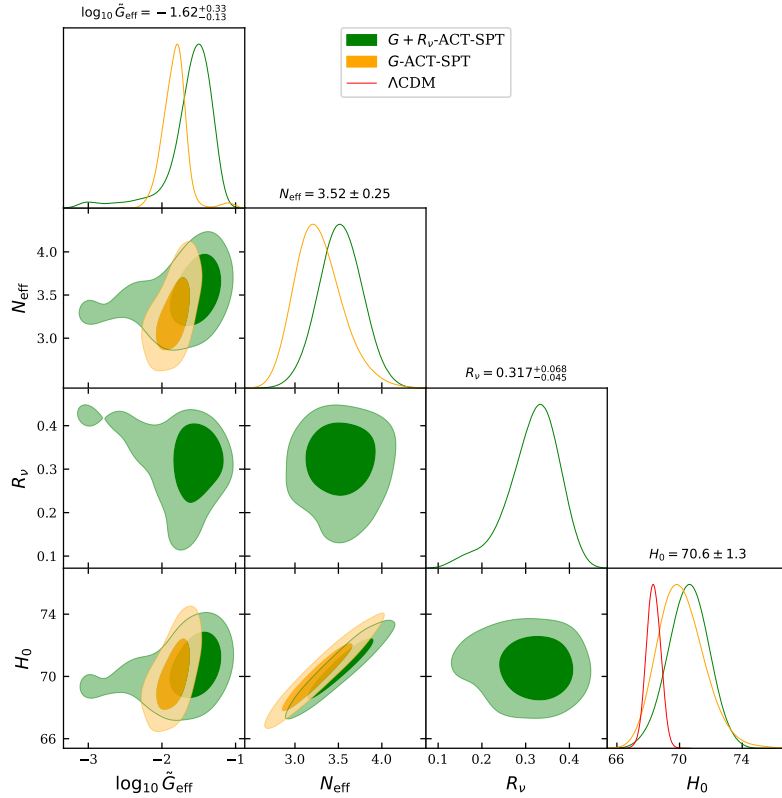


Figure 8. The posterior one-dimension distribution for parameter constraints when combining baseline dataset with ACT and SPT.

Innovation Team (JCTD-2022-20), NSFC (12261131497, 11653002), 111 Project for “Observational and Theoretical Research on Dark Matter and Dark Energy” (B23042), Fundamental Research Funds for Central Universities, CSC Innovation Talent Funds, USTC Fellowship for International Cooperation, USTC Research Funds of the Double First-Class Initiative, CAS project for young scientists in basic research (YSBR-006). We acknowledge the use of computing facilities of astronomy department, as well as the clusters LINDA & JUDY of the particle cosmology group at USTC.

References

- [1] A.G. Riess et al., *A 2.4% Determination of the Local Value of the Hubble Constant*, *Astrophys. J.* **826** (2016) 56 [[1604.01424](#)].
- [2] PLANCK collaboration, *Planck 2013 results. XVI. Cosmological parameters*, *Astron. Astrophys.* **571** (2014) A16 [[1303.5076](#)].
- [3] J.L. Bernal, L. Verde and A.G. Riess, *The trouble with H_0* , *JCAP* **10** (2016) 019 [[1607.05617](#)].
- [4] W.L. Freedman, *Cosmology at a Crossroads*, *Nature Astron.* **1** (2017) 0121 [[1706.02739](#)].

Parameter 68%	G ACT-SPT	$G + R_\nu$ ACT-SPT
$\log(10^{10} A_s)$	$2.973^{+0.017}_{-0.014}$	3.025 ± 0.018
n_s	$0.9320^{+0.0069}_{-0.0052}$	0.9555 ± 0.0078
$\Omega_b h^2$	0.02232 ± 0.00017	0.02227 ± 0.00015
$\Omega_c h^2$	$0.1249^{+0.0041}_{-0.0056}$	0.1275 ± 0.0044
τ_{reio}	$0.0485^{+0.0075}_{-0.0064}$	0.0489 ± 0.0069
H_0	$70.1^{+1.3}_{-1.6}$	70.6 ± 1.3
$\log_{10} G_{\text{eff}}$	-1.82 ± 0.18	-1.82 ± 0.18
N_{eff}	$3.27^{+0.23}_{-0.31}$	3.52 ± 0.25
Ω_m	0.2996 ± 0.0055	0.3007 ± 0.0055
S_8	0.834 ± 0.012	0.831 ± 0.011
R_ν	0	$0.317^{+0.068}_{-0.045}$
R_x	-	$0.127^{+0.047}_{-0.068}$
$\Delta\chi^2_{\text{Planck}}$	8.1	2.9
$\Delta\chi^2_{\text{base}}$	4.3	-3.0

Table 4. The best fit and 1σ error of the parameters using baseline dataset with ACT and SPT.

- [5] PLANCK collaboration, *Planck intermediate results. XLVI. Reduction of large-scale systematic effects in HFI polarization maps and estimation of the reionization optical depth*, *Astron. Astrophys.* **596** (2016) A107 [[1605.02985](#)].
- [6] E. Di Valentino, O. Mena, S. Pan, L. Visinelli, W. Yang, A. Melchiorri et al., *In the realm of the Hubble tension—a review of solutions*, *Class. Quant. Grav.* **38** (2021) 153001 [[2103.01183](#)].
- [7] V. Poulin, T.L. Smith and T. Karwal, *The Ups and Downs of Early Dark Energy solutions to the Hubble tension: a review of models, hints and constraints circa 2023*, [2302.09032](#).
- [8] C. Heymans et al., *KiDS-1000 Cosmology: Multi-probe weak gravitational lensing and spectroscopic galaxy clustering constraints*, *Astron. Astrophys.* **646** (2021) A140 [[2007.15632](#)].
- [9] J.C. Hill, E. McDonough, M.W. Toomey and S. Alexander, *Early dark energy does not restore cosmological concordance*, *Phys. Rev. D* **102** (2020) 043507 [[2003.07355](#)].
- [10] L. Ackerman, M.R. Buckley, S.M. Carroll and M. Kamionkowski, *Dark Matter and Dark Radiation*, *Phys. Rev. D* **79** (2009) 023519 [[0810.5126](#)].
- [11] S. Kumar, R.C. Nunes and S.K. Yadav, *Cosmological bounds on dark matter-photon coupling*, *Phys. Rev. D* **98** (2018) 043521 [[1803.10229](#)].
- [12] S. Ghosh, R. Khatri and T.S. Roy, *Can dark neutrino interactions phase out the Hubble tension?*, *Phys. Rev. D* **102** (2020) 123544 [[1908.09843](#)].
- [13] G. Mangano, G. Miele, S. Pastor, T. Pinto, O. Pisanti and P.D. Serpico, *Relic neutrino decoupling including flavour oscillations*, *Nuclear Physics B* **729** (2005) 221.
- [14] S. Vagnozzi, *New physics in light of the H_0 tension: An alternative view*, *Phys. Rev. D* **102** (2020) 023518 [[1907.07569](#)].
- [15] L.A. Anchordoqui, H. Goldberg and G. Steigman, *Right-Handed Neutrinos as the Dark Radiation: Status and Forecasts for the LHC*, *Phys. Lett. B* **718** (2013) 1162 [[1211.0186](#)].
- [16] T.D. Jacques, L.M. Krauss and C. Lunardini, *Additional Light Sterile Neutrinos and Cosmology*, *Phys. Rev. D* **87** (2013) 083515 [[1301.3119](#)].
- [17] C.D. Kreisch, F.-Y. Cyr-Racine and O. Doré, *Neutrino puzzle: Anomalies, interactions, and cosmological tensions*, *Phys. Rev. D* **101** (2020) 123505 [[1902.00534](#)].

- [18] I.M. Oldengott, C. Rampf and Y.Y.Y. Wong, *Boltzmann hierarchy for interacting neutrinos I: formalism*, *JCAP* **04** (2015) 016 [[1409.1577](#)].
- [19] F. D’Eramo, R.Z. Ferreira, A. Notari and J.L. Bernal, *Hot Axions and the H_0 tension*, *JCAP* **11** (2018) 014 [[1808.07430](#)].
- [20] V. Poulin, T.L. Smith, D. Grin, T. Karwal and M. Kamionkowski, *Cosmological implications of ultralight axionlike fields*, *Phys. Rev. D* **98** (2018) 083525 [[1806.10608](#)].
- [21] Z. Hou, R. Keisler, L. Knox, M. Millea and C. Reichardt, *How Massless Neutrinos Affect the Cosmic Microwave Background Damping Tail*, *Phys. Rev. D* **87** (2013) 083008 [[1104.2333](#)].
- [22] R.-Y. Guo and X. Zhang, *Constraints on inflation revisited: An analysis including the latest local measurement of the Hubble constant*, *Eur. Phys. J. C* **77** (2017) 882 [[1704.04784](#)].
- [23] T. Tram, R. Vallance and V. Vennin, *Inflation Model Selection meets Dark Radiation*, *JCAP* **01** (2017) 046 [[1606.09199](#)].
- [24] M. Escudero, *Neutrino decoupling beyond the Standard Model: CMB constraints on the Dark Matter mass with a fast and precise N_{eff} evaluation*, *JCAP* **02** (2019) 007 [[1812.05605](#)].
- [25] J.M. Conrad, C.M. Ignarra, G. Karagiorgi, M.H. Shaevitz and J. Spitz, *Sterile Neutrino Fits to Short Baseline Neutrino Oscillation Measurements*, *Adv. High Energy Phys.* **2013** (2013) 163897 [[1207.4765](#)].
- [26] M. Archidiacono, E. Calabrese and A. Melchiorri, *The Case for Dark Radiation*, *Phys. Rev. D* **84** (2011) 123008 [[1109.2767](#)].
- [27] M. Archidiacono, S. Gariazzo, C. Giunti, S. Hannestad, R. Hansen, M. Laveder et al., *Pseudoscalar—sterile neutrino interactions: reconciling the cosmos with neutrino oscillations*, *JCAP* **08** (2016) 067 [[1606.07673](#)].
- [28] M. Archidiacono, S. Hannestad, R.S. Hansen and T. Tram, *Cosmology with self-interacting sterile neutrinos and dark matter - A pseudoscalar model*, *Phys. Rev. D* **91** (2015) 065021 [[1404.5915](#)].
- [29] X. Chu, B. Dasgupta and J. Kopp, *Sterile neutrinos with secret interactions—lasting friendship with cosmology*, *JCAP* **10** (2015) 011 [[1505.02795](#)].
- [30] T. Brinckmann, J.H. Chang and M. LoVerde, *Self-interacting neutrinos, the Hubble parameter tension, and the cosmic microwave background*, *Phys. Rev. D* **104** (2021) 063523 [[2012.11830](#)].
- [31] M. Zaldarriaga and D.D. Harari, *Analytic approach to the polarization of the cosmic microwave background in flat and open universes*, *Phys. Rev. D* **52** (1995) 3276 [[astro-ph/9504085](#)].
- [32] S. Bashinsky and U. Seljak, *Neutrino perturbations in CMB anisotropy and matter clustering*, *Phys. Rev. D* **69** (2004) 083002 [[astro-ph/0310198](#)].
- [33] D. Baumann, D. Green, J. Meyers and B. Wallisch, *Phases of New Physics in the CMB*, *JCAP* **01** (2016) 007 [[1508.06342](#)].
- [34] B. Follin, L. Knox, M. Millea and Z. Pan, *First Detection of the Acoustic Oscillation Phase Shift Expected from the Cosmic Neutrino Background*, *Phys. Rev. Lett.* **115** (2015) 091301 [[1503.07863](#)].
- [35] D. Baumann, D. Green and B. Wallisch, *Searching for light relics with large-scale structure*, *JCAP* **08** (2018) 029 [[1712.08067](#)].
- [36] D. Baumann, D. Green and M. Zaldarriaga, *Phases of New Physics in the BAO Spectrum*, *JCAP* **11** (2017) 007 [[1703.00894](#)].
- [37] D.D. Baumann, F. Beutler, R. Flauger, D.R. Green, A. Slosar, M. Vargas-Magaña et al., *First constraint on the neutrino-induced phase shift in the spectrum of baryon acoustic oscillations*, *Nature Phys.* **15** (2019) 465 [[1803.10741](#)].

- [38] D. Blas, J. Lesgourgues and T. Tram, *The Cosmic Linear Anisotropy Solving System (CLASS) II: Approximation schemes*, *JCAP* **07** (2011) 034 [[1104.2933](#)].
- [39] K.M. Nollett and G. Steigman, *BBN And The CMB Constrain Light, Electromagnetically Coupled WIMPs*, *Phys. Rev. D* **89** (2014) 083508 [[1312.5725](#)].
- [40] C. Benso, W. Rodejohann, M. Sen and A.U. Ramachandran, *Sterile neutrino dark matter production in presence of nonstandard neutrino self-interactions: An EFT approach*, *Phys. Rev. D* **105** (2022) 055016 [[2112.00758](#)].
- [41] A. De Gouvêa, M. Sen, W. Tangarife and Y. Zhang, *Dodelson-Widrow Mechanism in the Presence of Self-Interacting Neutrinos*, *Phys. Rev. Lett.* **124** (2020) 081802 [[1910.04901](#)].
- [42] A. Merle, A. Schneider and M. Totzauer, *Dodelson-Widrow Production of Sterile Neutrino Dark Matter with Non-Trivial Initial Abundance*, *JCAP* **04** (2016) 003 [[1512.05369](#)].
- [43] F. De Bernardis, L. Pagano, P. Serra, A. Melchiorri and A. Cooray, *Anisotropies in the Cosmic Neutrino Background after WMAP 5-year Data*, *JCAP* **06** (2008) 013 [[0804.1925](#)].
- [44] G. Mangano, G. Miele, S. Pastor, T. Pinto, O. Pisanti and P.D. Serpico, *Relic neutrino decoupling including flavor oscillations*, *Nucl. Phys. B* **729** (2005) 221 [[hep-ph/0506164](#)].
- [45] W. Hu and N. Sugiyama, *Anisotropies in the cosmic microwave background: An Analytic approach*, *Astrophys. J.* **444** (1995) 489 [[astro-ph/9407093](#)].
- [46] M.-X. Lin, M. Raveri and W. Hu, *Phenomenology of Modified Gravity at Recombination*, *Phys. Rev. D* **99** (2019) 043514 [[1810.02333](#)].
- [47] S. Bashinsky and U.c.v. Seljak, *Signatures of relativistic neutrinos in cmb anisotropy and matter clustering*, *Phys. Rev. D* **69** (2004) 083002.
- [48] G. Choi, C.-T. Chiang and M. LoVerde, *Probing Decoupling in Dark Sectors with the Cosmic Microwave Background*, *JCAP* **06** (2018) 044 [[1804.10180](#)].
- [49] F.-Y. Cyr-Racine and K. Sigurdson, *Limits on Neutrino-Neutrino Scattering in the Early Universe*, *Phys. Rev. D* **90** (2014) 123533 [[1306.1536](#)].
- [50] C.-P. Ma and E. Bertschinger, *Cosmological perturbation theory in the synchronous and conformal Newtonian gauges*, *Astrophys. J.* **455** (1995) 7 [[astro-ph/9506072](#)].
- [51] A. Das and S. Ghosh, *The magnificent ACT of flavor-specific neutrino self-interaction*, [2303.08843](#).
- [52] J. Torrado and A. Lewis, *Cobaya: Code for Bayesian Analysis of hierarchical physical models*, *JCAP* **05** (2021) 057 [[2005.05290](#)].
- [53] A. Gelman and D.B. Rubin, *Inference from Iterative Simulation Using Multiple Sequences*, *Statist. Sci.* **7** (1992) 457.
- [54] PLANCK collaboration, *Planck 2018 results. V. CMB power spectra and likelihoods*, *Astron. Astrophys.* **641** (2020) A5 [[1907.12875](#)].
- [55] A.G. Riess et al., *New Parallaxes of Galactic Cepheids from Spatially Scanning the Hubble Space Telescope: Implications for the Hubble Constant*, *Astrophys. J.* **855** (2018) 136 [[1801.01120](#)].
- [56] PAN-STARRS1 collaboration, *The Complete Light-curve Sample of Spectroscopically Confirmed SNe Ia from Pan-STARRS1 and Cosmological Constraints from the Combined Pantheon Sample*, *Astrophys. J.* **859** (2018) 101 [[1710.00845](#)].
- [57] F. Beutler, C. Blake, M. Colless, D.H. Jones, L. Staveley-Smith, L. Campbell et al., *The 6dF Galaxy Survey: Baryon Acoustic Oscillations and the Local Hubble Constant*, *Mon. Not. Roy. Astron. Soc.* **416** (2011) 3017 [[1106.3366](#)].

- [58] A.J. Ross, L. Samushia, C. Howlett, W.J. Percival, A. Burden and M. Manera, *The clustering of the SDSS DR7 main Galaxy sample – I. A 4 per cent distance measure at $z = 0.15$* , *Mon. Not. Roy. Astron. Soc.* **449** (2015) 835 [[1409.3242](#)].
- [59] BOSS collaboration, *The clustering of galaxies in the completed SDSS-III Baryon Oscillation Spectroscopic Survey: cosmological analysis of the DR12 galaxy sample*, *Mon. Not. Roy. Astron. Soc.* **470** (2017) 2617 [[1607.03155](#)].
- [60] ACT collaboration, *The Atacama Cosmology Telescope: DR4 Maps and Cosmological Parameters*, *JCAP* **12** (2020) 047 [[2007.07288](#)].
- [61] ACT collaboration, *The Atacama Cosmology Telescope: a measurement of the Cosmic Microwave Background power spectra at 98 and 150 GHz*, *JCAP* **12** (2020) 045 [[2007.07289](#)].
- [62] SPT-3G collaboration, *Measurements of the E-mode polarization and temperature-E-mode correlation of the CMB from SPT-3G 2018 data*, *Phys. Rev. D* **104** (2021) 022003 [[2101.01684](#)].
- [63] S. Dodelson, *Modern Cosmology*, Academic Press, Amsterdam (2003).
- [64] W.L.K. Wu, J. Errard, C. Dvorkin, C.L. Kuo, A.T. Lee, P. McDonald et al., *A guide to designing future ground-based cmb experiments*, *The Astrophysical Journal* **788** (2014) 138 [[1402.4108](#)].
- [65] W. Hu and T. Okamoto, *Mass reconstruction with cmb polarization*, *The Astrophysical Journal* **574** (2002) 566 [[astro-ph/0111606](#)].
- [66] Z. Li, V. Gluscevic, K.K. Boddy and M.S. Madhavacheril, *Disentangling Dark Physics with Cosmic Microwave Background Experiments*, *Phys. Rev. D* **98** (2018) 123524 [[1806.10165](#)].
- [67] Y.-P. Li, Y. Liu, S.-Y. Li, H. Li and X. Zhang, *Tibet’s Ali: A New Window to Detect the CMB Polarization*, [1709.09053](#).
- [68] C.-L. Kuo, *Assessments of Ali, Dome A, and Summit Camp for Mm-wave Observations Using MERRA-2 Reanalysis*, *Astrophys. J.* **848** (2017) 64 [[1707.08400](#)].
- [69] H. Li, S.-Y. Li, Y. Liu, Y.-P. Li and X. Zhang, *Tibet’s window on primordial gravitational waves*, *Nature Astron.* **2** (2018) 104 [[1802.08455](#)].
- [70] M. Salatino et al., *The design of the Ali CMB Polarization Telescope receiver*, *Proc. SPIE Int. Soc. Opt. Eng.* **11453** (2020) 114532A [[2101.09608](#)].
- [71] Y.-F. Cai and X. Zhang, *Probing the origin of our universe through primordial gravitational waves by Ali CMB project*, *Sci. China Phys. Mech. Astron.* **59** (2016) 670431 [[1605.01840](#)].
- [72] H. Li et al., *Probing Primordial Gravitational Waves: Ali CMB Polarization Telescope*, *Natl. Sci. Rev.* **6** (2019) 145 [[1710.03047](#)].
- [73] D. Wu, H. Li, S. Ni, Z.-W. Li and C.-Z. Liu, *Detecting Primordial Gravitational Waves: a forecast study on optimizing frequency distribution of next generation ground-based CMB telescope*, *Eur. Phys. J. C* **80** (2020) 139.
- [74] Z. Zhang, Y. Liu, S.-Y. Li, D.-L. Wu, H. Li and H. Li, *Efficient ILC analysis on polarization maps after EB leakage correction*, *JCAP* **22** (2020) 044 [[2109.12619](#)].
- [75] J.-R. Li, C. Li, J. Jiang, Y.-F. Cai, J. Delabrouille, D. Wu et al., *CMB polarization analysis on circular scans*, *JCAP* **08** (2021) 033 [[2103.00561](#)].
- [76] J. Liu et al., *Forecasts on CMB lensing observations with AliCPT-1*, *Sci. China Phys. Mech. Astron.* **65** (2022) 109511 [[2204.08158](#)].
- [77] D. Zhang, J.-R. Li, J. Li, J. Yang, Y. Zhang, Y.-F. Cai et al., *Future Prospects on Constraining Neutrino Cosmology with the Ali CMB Polarization Telescope*, *Astrophys. J.* **946** (2023) 32 [[2112.10539](#)].

- [78] Y.-W. Wu, S. Li, Y. Liu, Z. Zhang, H. Liu and H. Li, *Study on the filters of atmospheric contamination in ground based CMB observation*, *JCAP* **04** (2023) 047 [[2210.09711](#)].
- [79] CMB-S4 collaboration, *CMB-S4 Science Book, First Edition*, [1610.02743](#).
- [80] A. Das and S. Ghosh, *Flavor-specific interaction favors strong neutrino self-coupling in the early universe*, *JCAP* **07** (2021) 038 [[2011.12315](#)].